Appl. Phys. A 68, 321–324 (1999)

Applied Physics A
Materials
Science & Processing
© Springer-Verlag 1999

Praseodymium-doped Ti:$LiNbO_3$ waveguides

I. Baumann[1,*], F. Cusso[2], B. Herreros[2], H. Holzbrecher[3], H. Paulus[4], K. Schäfer[1], W. Sohler[1]

[1] Universität-GH Paderborn, FB6 - Angewandte Physik, Warburger Str. 100, 33098 Paderborn, Germany
[2] Departamento de Fisica de Materiales, Universidad Autonoma de Madrid, 28049 Madrid, Spain
[3] Institut für Schicht- und Ionentechnik ISI, Forschungszentrum Jülich, 52425 Jülich, Germany
[4] Institut für Technologie- und Wissenstransfer im Kreis Soest, FB Elektrische Energietechnik der Universität-GH Paderborn, Abt. Soest, Steingraben 21, 59494 Soest, Germany

Received: 17 September 1998/Accepted: 11 November 1998

Abstract. The incorporation of praseodymium into $LiNbO_3$ by diffusion doping is investigated by means of secondary neutral mass spectrometry and secondary ion mass spectrometry. The diffusion of praseodymium in $LiNbO_3$ can be described by Fick's laws of diffusion with a concentration-independent diffusion coefficient and a limited solubility of praseodymium in $LiNbO_3$ increasing exponentially with rising temperature. The diffusion depends on the Li_2O content of the $LiNbO_3$ crystal. For $LiNbO_3$ crystals with a nominal slight difference in the congruent composition, the diffusion constants and activation energies for Z-cut $LiNbO_3$ are $3.28 \times 10^{-5}\,cm^2/s$ and 2.27 eV, and $1.39 \times 10^{-5}\,cm^2/s$ and 2.24 eV, respectively. Titanium-doped waveguides are formed in Pr:$LiNbO_3$ and characterised in relation to waveguide loss and absorption in the visible and near infrared.

PACS: 42.70; 66.30

Lithium niobate ($LiNbO_3$) is one of the most attractive materials for integrated optics due to its unique combination of excellent electrooptical, acoustooptical and non-linear optical properties. It opens the possibility of fabricating optically pumped waveguide amplifiers and lasers by doping a $LiNbO_3$ substrate with rare earth ions (Er, Nd, Yb, Tm) [1–4]. The rich optical spectrum of praseodymium extending from the ultraviolet to the near infrared enables the design of up-conversion lasers generating light in the visible, as well as amplifiers for optical communications in the wavelength range around $\lambda = 1.3\,\mu m$ [5–7].

This paper reports for the first time on praseodymium doping of $LiNbO_3$ by in-diffusion. This is a simple and efficient technique yielding highly doped surface layers of excellent optical quality allowing the fabrication of low-loss optical channel waveguides by titanium in-diffusion. The diffusion constants and the maximum solubility of Pr in $LiNbO_3$ were determined by analysing Pr doping profiles using SNMS (secondary neutral mass spectrometry) and SIMS (secondary ion mass spectrometry). A knowledge of the diffusion constants and of the solubility of Pr is necessary for the fabrication of Ti:Pr:$LiNbO_3$ waveguides with optimised overlap of the Pr doping profile and the intensity distribution of the guided optical modes. A first characterisation of Ti-doped waveguides in Pr:$LiNbO_3$ is presented.

1 Experiment

Two sets of samples were prepared using Z-cut $LiNbO_3$ wafers grown from congruent melts by different suppliers: $LiNbO_3$ wafers produced by Crystal Technology Inc. (CTI) with a composition of 48.38 mol % Li_2O [8] and wafers from Telefilter (tft) with 48.47 mol % Li_2O [9]. The congruent composition is needed to allow the growth of compositionally and optically homogeneous $LiNbO_3$ crystals. The quantitative figure of the congruent composition depends on the crystal growth conditions. The real point defect structure of $LiNbO_3$ depends on the given Li/Nb ratio of the melt and on the given growth conditions [10].

For the determination of the diffusion coefficients and the solubility of praseodymium in $LiNbO_3$ a metallic Pr layer of 17.1 nm thickness was deposited on the surface of the samples by electron beam evaporation at 6×10^{-5} Pa resulting in a Pr surface coverage of $(5.0 \pm 0.2) \times 10^{16}\,cm^{-2}$. The diffusion was carried out in a platinum box at temperatures/durations of 1030 °C/50 h, 1100 °C/40 h and 1130 °C/40 h for the samples from CTI and of 1030 °C/50 h and 1065 °C/50 h for the samples from tft, respectively. During the first two hours the diffusion was performed in a dry oxygen atmosphere to fully oxidise the Pr layer followed by a diffusion in argon atmosphere. During the last hour the diffusion was carried out again in an oxygen atmosphere to compensate the loss of oxygen of the crystal.

An additional set of Z-cut $LiNbO_3$ samples from CTI was prepared to get Ti-doped channel waveguides in doped Pr:$LiNbO_3$. Praseodymium layers of 14.5 nm and 17.2 nm thickness were in-diffused at 1130 °C/150 h followed by the in-diffusion (1060 °C/5 h) of 5, 6 and 7 μm wide, photolitho-

* *Present address*:SIEMENS AG, Abt. HL FO E S, Wernerwerkstr. 2, 93049 Regenburg, Germany

graphically defined Ti stripes of 74 nm thickness. The length of the waveguides was 51 and 54 mm, respectively.

To analyse the concentration profile of the in-diffused Pr quantitatively with high accuracy, both SNMS and SIMS were used. Details of the methods are described in [11]. SNMS measurements were performed with the high frequency mode (HFM) on a Specs INA-3 machine. Using HFM-SNMS with 700 V acceleration voltage at 320 kHz a sputter rate of about 0.6 nm/s was achieved. The detection sensitivity of Pr in $LiNbO_3$ using SNMS was 50 ppm. SIMS measurements used to analyse deep concentration profiles were performed with a CAMECA-IMS4F instrument. An O^{2+}-beam of 500 nA at 5.5 keV was used to sputter a crater of $200 \times 200\,\mu m^2$ cross section at a rate of about 1 nm/s. The detection sensitivity for Pr in $LiNbO_3$ using SIMS was 8 ppm.

The measured Pr concentration profiles were normalised to the oxygen as well as to the niobium signal (SNMS) and to the niobium signal only (SIMS). The quantitative determination of the Pr concentration was performed using the law of mass conservation. The depth of the craters was measured by a depth profiler and a linear time versus depth relationship was assumed for the sputter process.

The total losses of the channel waveguides were measured using the low finesse method [12]. Absorption in the Pr-doped channels was investigated in the visible (500–800 nm) and the near infrared (1000–1700 nm) without polarisation control using a white light source and a monochromator with spectral resolution of about 1 nm. The light was butt-coupled into the waveguides using a 1.3 μm standard single mode fiber. At the output of the Ti:Pr:$LiNbO_3$ waveguide a second 1.3 μm standard single mode fiber was used connected to the detector unit, a liquid nitrogen cooled Ge detector and a photomultiplier R928 HFT (Hamamatsu), respectively.

2 Results and discussion

2.1 *Diffusivity and solubility of* Pr *in* $LiNbO_3$

Assuming a concentration-independent diffusion coefficient of Pr, D_{Pr}, concentration profiles resulting from planar doping can be derived from the one-dimensional diffusion equation corresponding to Fick's law. Taking into account a finite solid solubility of Pr in $LiNbO_3$ the Pr concentration at the surface of the substrate, $c_{Pr,0}$, remains constant as long as the Pr reservoir is not depleted. The corresponding solution is a complementary error function [13]:

$$c_{Pr}(y, t) = c_{Pr,0}\,\mathrm{erfc}\left(\frac{y}{2\sqrt{D_{Pr}t}}\right) , \qquad (1)$$

where $c_{Pr,0}$ corresponds to the temperature dependent solid solubility of Pr in $LiNbO_3$. For long diffusion times the diffusion reservoir at the surface is depleted and the solution of the diffusion equation can be approximated by a Gaussian distribution for the Pr concentration (for more details see [14]).

The unambiguous determination of the diffusion coefficients *and* the solubility is only possible using Pr concentration profiles corresponding to (1). Some of the Pr concentration profiles obtained by SNMS are shown in Fig. 1. A Pr-rich surface layer also containing Nb, Li and O of about 100–150 nm thickness was observed on the surface of the substrates (shown in the inset of the figure); it represents the undepleted diffusion reservoir. A detailed compositional phase analysis is necessary to describe the phases formed in this layer. The doping profile suggests a Pr distribution corresponding to (1). The transitions between the Pr-rich surface compounds and the concentration profiles correspond to the maximum solubility of Pr in $LiNbO_3$ at the given diffusion temperatures. The concentration profiles of Pr in the inset reveal that the diffusion is different using different nominal congruent compositions.

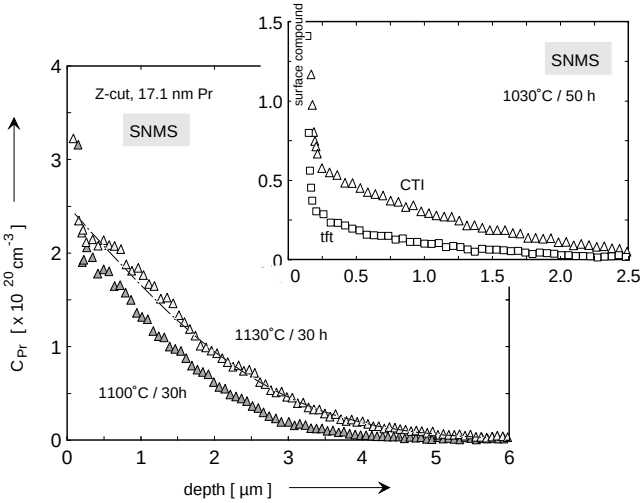

Fig. 1. Praseodymium doping profiles obtained by SNMS for different diffusion temperatures (1030 °C ≤ T_{diff} ≤ 1130 °C). The *dash-dotted line* reveals a fit corresponding to (1). Due to the chosen experimental conditions for the Pr diffusion the reservoir at the surface is not completely depleted. A thin surface compound consisting of a Pr-rich niobium-lithium-oxide of about 100–150 nm thickness remains at the surface. The inset reveals the dependence of the diffusivity of Pr on the Li_2O content (*triangles* - $LiNbO_3$ from CTI: 48.38 mol % Li_2O; *squares* - $LiNbO_3$ from tft: 48.47 mol % Li_2O)

Least square fits of complementary error functions corresponding to (1) give a good agreement with the measured doping profiles below the surface compound. The parameters of the fits yield the diffusion coefficients and the solubility data. The main uncertainties in these data result from the signal-to-noise ratio of the measurement influenced by NbO_3 having the same mass number as Pr and from the limited accuracy of the depth scaling. The accuracy of the diffusion coefficients is given by $\pm 2 \times 10^{-15}\,cm^2/s$ and $\pm 1.5 \times 10^{-14}\,cm^2/s$ for the diffusion at 1030 °C and 1130 °C, respectively.

SIMS analysis of Pr depth profiles resulting from the diffusion at 1100 °C/150 h and 1130 °C/150 h confirms the results of the determination of the diffusion coefficients obtained by SNMS.

The Arrhenius plots in Fig. 2 summarise the results. The diffusion constant is clearly dependent on the composition of the $LiNbO_3$ substrate; a slight increase of the Li_2O content decreases the diffusivity. The diffusion coefficients are well-fitted by

$$D_{Pr} = D_{Pr,0}\,\exp\left(-\frac{E_a}{k_B T}\right) , \qquad (2)$$

as shown by the dash-dotted lines in Fig. 2, k_B is Boltzmann's constant and T is the absolute diffusion temperature. The

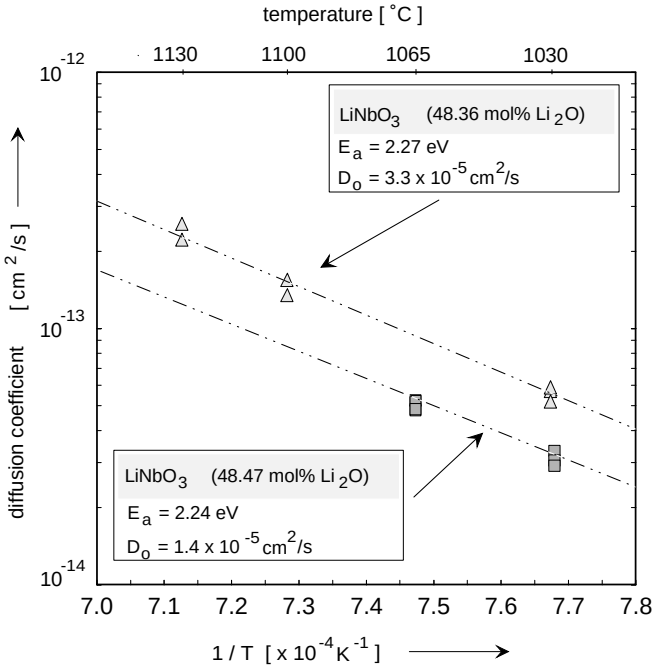

Fig. 2. Arrhenius plot of the diffusion coefficients of praseodymium in $LiNbO_3$ for diffusion parallel to the *c*-axis (Z-cut) of $LiNbO_3$ measured by SNMS. The *dash-dotted line* shows a fit corresponding to (2). (*triangles* - $LiNbO_3$ from CTI: 48.38 mol % Li_2O; *squares* - $LiNbO_3$ from tft: 48.47 mol % Li_2O)

diffusion constant $D_{\mathrm{Pr},0}$ and activation energy E_a are $(3.3 \pm 0.5) \times 10^{-5}\,\mathrm{cm}^2/\mathrm{s}$ and $(2.27 \pm 0.08)\,\mathrm{eV}$ for $LiNbO_3$ from CTI with 48.36 mol % Li_2O and $(1.4 \pm 0.5) \times 10^{-5}\,\mathrm{cm}^2/\mathrm{s}$ and $(2.24 \pm 0.08)\,\mathrm{eV}$ for $LiNbO_3$ from tft with 48.47 mol % Li_2O.

The solubility of Pr in $LiNbO_3$ is presented in Fig. 3 as function of temperature. The main behavior is nearly the same as observed for erbium in $LiNbO_3$ [11]. In systems of very limited solubility an exponential law describes the rise of the solubility with temperature:

$$c_{\mathrm{Pr},0} = c_{\mathrm{Pr,s}} \exp\left(-\frac{\Delta H_\mathrm{s}}{k_\mathrm{B} T}\right) , \tag{3}$$

where ΔH_s is the heat of solution and $c_{\mathrm{Pr,s}}$ is the solubility constant [15]. A dependence on the composition of the substrate material is observed again; the higher amount of Li_2O in the tft sample reduces the Pr solubility. The Arrhenius plots of the solubility data fit well with (3). For the CTI material, $\Delta H_\mathrm{s} = 2.38\,\mathrm{eV}$ and $c_{\mathrm{Pr,s}} = 1.0 \times 10^{29}\,\mathrm{cm}^{-3}$ and for the tft material $\Delta H_\mathrm{s} = 2.18\,\mathrm{eV}$ and $c_{\mathrm{Pr,s}} = 9.5 \times 10^{27}\,\mathrm{cm}^{-3}$ were found.

The activation energy for diffusion is the energy required to surmount the barrier between adjacent lattice sites suitable for migration as well as for incorporation of a dopant. The figures for E_a for the two materials are nearly equal. The difference in the diffusivity results from D_0 which depends on the jump-attempt frequency, the jump distance, and the concentration and location of vacancies in the lattice. The higher the amount of Li_2O in the $LiNbO_3$ crystal, i.e. the closer the composition is to stoichiometry, the lower becomes the number of suitable vacancies for migration and incorporation. This reduces the diffusivity and the solubility, too. This dependence of the diffusivity of Pr on the $LiNbO_3$ host composition is similar to that observed by Holmes et al. for Ti in $LiNbO_3$ [16].

Comparing the results of the diffusivity and solubility of Pr in $LiNbO_3$ with those of [11] reveals nearly equal activation energy (for Er in $LiNbO_3$ (Z-cut) $E_\mathrm{a} = 2.28\,\mathrm{eV}$ [8]) but a lower diffusivity of Pr. Due to the similar chemical behavior of Er and Pr, the reduced diffusivity of Pr can be attributed to its higher ionic radius. This induces additional strain in the crystal structure of the host, decreasing the jump-attempt frequency [15]. The reduced solubility is also attributed to the size factor.

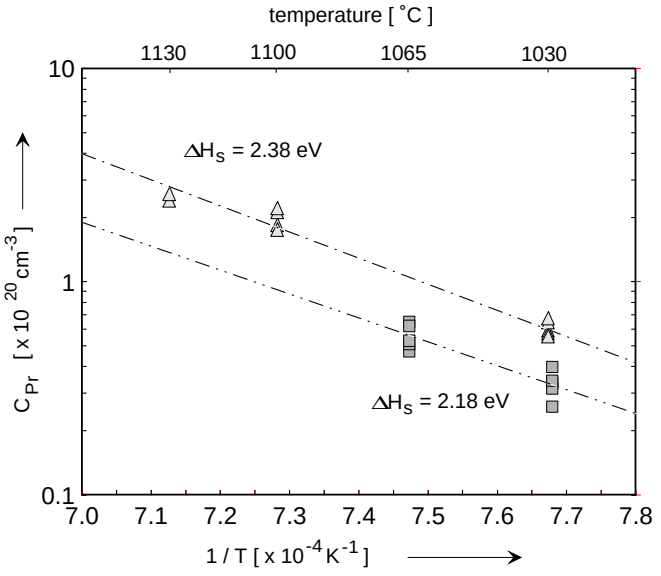

Fig. 3. Arrhenius plot of the solubility data of praseodymium in $LiNbO_3$ revealing the exponential increase of the solubility with rising temperature. (ΔH_s - heat of solution) (*triangles* - $LiNbO_3$ from CTI: 48.38 mol % Li_2O; *squares* - $LiNbO_3$ from tft: 48.47 mol % Li_2O)

2.2 Characterisation of Ti*:* Pr*:* $LiNbO_3$ *channel waveguides*

Optical characterisation of the Ti:Pr:$LiNbO_3$ channel waveguides proved that the 6 μm (7 μm) wide channels are single mode in the wavelength range from 1190 nm (1310 nm) to 1700 nm, respectively. The intensity distribution of the guided modes in 7 μm wide channels was $6.6\,\mu\mathrm{m} \times 4.6\,\mu\mathrm{m}$ (TE) and $4.7\,\mu\mathrm{m} \times 2.8\,\mu\mathrm{m}$ (TM) full width at half maximum at 1546 nm. The total losses of the undoped channels were $(0.03 \pm 0.01)\,\mathrm{dB/cm}$ (TE) and $(0.07 \pm 0.02)\,\mathrm{dB/cm}$ (TM). With the knowledge of the unpolarised absorption and the measurement of the total losses of doped channels at 1523 nm, scattering losses of 0.10–0.15 dB/cm ($\pm 0.05\,\mathrm{dB/cm}$) were estimated for the doped channels.

Figure 4 shows the room temperature absorption of a Ti:Pr:$LiNbO_3$ waveguide (14.5 nm Pr, 1130 °C, 150 h, 7 μm wide channel) measured in the range of $500\,\mathrm{nm} \leq \lambda \leq 1700\,\mathrm{nm}$. Up to 1310 nm wavelength the waveguide is multimode as shown by the oscillation of the transmission signal. In the wavelength range 500–800 nm, due to transitions from the ground state, the $^3P_1$, $^3P_0$ and $^1D_2$ levels are detected. The weak $^1G_4$ absorption level at about 1030 nm was not detectable in this waveguide due to the multi-mode oscillations. In the range 1310–1700 nm the Ti-doped waveguide is single

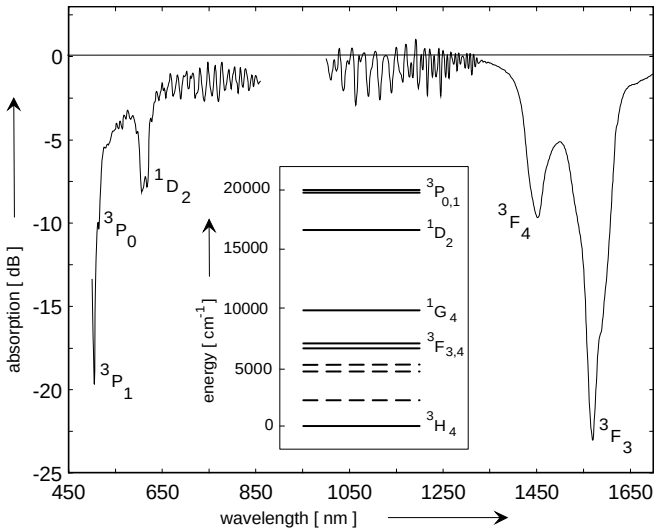

Fig. 4. Absorption spectra of a Ti:Pr:$LiNbO_3$ channel waveguide (Z-cut $LiNbO_3$; 14.5 nm Pr diffused at 1130 °C/150 h; 7 µm wide channel of 74 nm Ti diffused at 1060 °C/5 h). The strong oscillations below 1300 nm are due to the multi-mode behavior of the waveguide. *Inset*: Energy level scheme of Pr:$LiNbO_3$. *Full lines* - ground state and observed absorption bands, *dashed lines* - absorption bands at longer wavelength [14]

mode and the strong absorption bands due to the $^3F_4$ and $^3F_3$ energy levels can be seen. The absorption spectra obtained are in agreement with the results of bulk doped Pr:$LiNbO_3$ published by Lorenzo et al. [17].

Figure 5 shows the absorption of 5 µm wide channel waveguides with different doping levels. These waveguides are single mode in the range 1100–1700 nm. In spite of the multi-mode behavior for $\lambda < 1100$ nm, the $^1G_4$ absorption band is demonstrably present. The inset in Fig. 5 shows the corresponding absorption using a linear scale (multi-mode oscillations are removed by calculation). The resulting absorption is about 20% (1 dB).

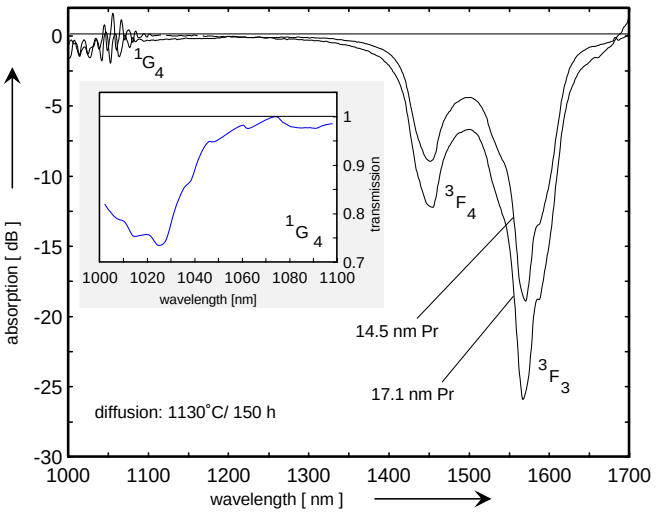

Fig. 5. Comparison of the absorption spectra of two 5 µm wide channel waveguides with different doping levels of praseodymium in $LiNbO_3$. (17.1 nm Pr and 14.5 nm Pr correspond to a praseodymium concentration of 7.58×10^{19} cm^{-3} and 6.37×10^{19} cm^{-3} Pr at 2 µm below the surface of the sample, respectively.) *Inset*: Weak $^1G_4$ absorption at about 1020 nm

The increase of the absorption with the increase with the doping level of praseodymium corresponds to the relation

$$T(\lambda, l) = \exp\left(-l\sigma_a(\lambda) \int N_0(x, y) s_0(x, y, \lambda)\, \mathrm{d}A\right) \qquad (4)$$

assuming a constant absorption cross section $\sigma_a(\lambda)$, where l is the length of the waveguide, $N_0(x, y)$ the concentration profile of praseodymium and $s_0(x, y, \lambda)$ is the optical intensity distribution of the guided mode. The structure observed inside the bands is mainly due to the splitting of the different levels in the crystal field by the Stark effect.

3 Conclusion

The diffusion of Pr into $LiNbO_3$ can be described by Fick's laws of diffusion with a concentration-independent diffusion coefficient and a temperature-dependent maximum solubility of Pr in $LiNbO_3$. The solubility of Pr grows exponentially with rising temperature. The diffusivity and solubility of Pr depend on the Li_2O content of the $LiNbO_3$ crystal, and are reduced with increasing Li_2O content. Using diffusion-doped Pr:$LiNbO_3$ the fabrication of low-loss Ti-doped channel waveguides is possible, but pumping via the $^1G_4$ energy level is not very efficient for amplifier and laser applications due to the low absorption. An enhancement of the pump efficiency can be obtained by Yb codoping of $LiNbO_3$ during the Pr-doping process [18].

References

1. I. Baumann, R. Brinkmann, M. Dinand, W. Sohler, S. Westenhöfer: IEEE J. Quantum Electron. **QE-32**(9), 1695 (1996)
2. E. Lallier, J.P. Pochelle, M. Papuchon, Q. He, M. de Micheli, B. Ostrowsky: Electron. Lett. **27**(11), 936 (1991)
3. J.K. Jones, J.P. deSandro, M. Hempstead, D.P. Shepherd, A.C. Larde, A.C. Tropper, J.S. Wilkinson: Opt. Lett. **20**(13), 1477 (1995)
4. J.P. deSandro, J.K. Jones, D.P. Shepherd, J. Webjörn, M. Hempstead, J. Wang, A.C. Tropper: Proc. 7th Europ. Conf. on Int. Opt. (ECIO'95), Delft, post-deadline papers 17
5. T. Sugawa, Y. Miyajima: IEEE Photon. Technol. Lett. **3**(7), 616 (1991)
6. Y. Ohishi, T. Kanamori, T. Nishi, N. Takahashi: IEEE Photon. Technol. Lett. **3**(8), 715 (1991)
7. Y. Nishida, M. Yamada, J. Temmyo, T. Kanamori, Y. Ohishi: IEEE Photon. Technol. Lett. **9**(8), 1096 (1997)
8. P.F. Bordui, R.G. Norwood, C.D. Bird, G.D. Glavert: J. Cryst. Growth **113**, 61 (1991)
9. I. Baumann, P. Rudolph, D. Krabe, R. Schalge: J. Cryst. Growth **128**, 903 (1993)
10. D.P. Birnie III: J. Mater. Sci. **28**, 302 (1993)
11. I. Baumann, R. Brinkmann, M. Dinand, W. Sohler, L. Beckers, Ch. Buchal, M. Fleuster, H. Holzbrecher. H. Paulus, K.-H. Müller, Th. Gog, G. Materlik, O. Witte, H. Stolz, W. von der Osten: Appl. Phys. A **64**, 33 (1997)
12. R. Regener, W. Sohler: Appl. Phys. B **36**, 143 (1985)
13. J. Crank: *The Mathematics of Diffusion* (Claderon Press, Oxford 1975)
14. M. Dinand: PhD Thesis, University of Paderborn 1995
15. A.H. Cottrell: *Theoretical Structural Metallurgy* (Arnold, London 1954)
16. R.J. Holmes, D.M. Smyth: J. Appl. Phys. **55**(10), 3531 (1984)
17. A. Lorenzo, L.E. Bausa, J. Garcia Sole: Phys. Rev. B **51**(23), 16 643 (1995)
18. J.S. Wang, E.M. Vogel, E. Snitzer, J.L. Jackel, V.L. da Silva, Y. Silberberg: J. Non-Cryst. Solids **178**, 109 (1994)